CHAPTER ONE HUNDRED SIXTY

A TURBULENT TRANSPORT MODEL OF COASTAL PROCESSES

Y. Peter Sheng*, Member ASCE

ABSTRACT

A second-order closure model of turbulent transport and recent model applications to some problems of practical importance in coastal engineering are presented. Particular examples considered are the turbulent wave boundary layer under a linear and a cnoidal wave; current-wave interaction within the bottom boundary layer; mixed layer dynamics; wind-driven currents in a channel. Comparisons are made between the computed results and field/laboratory data.

1. INTRODUCTION

Turbulent transport plays a dominant role in many coastal processes, e.g., sediment dispersion, wave-induced currents in the surf zone, and forces on structures. The accurate prediction of these processes requires a sound understanding of the turbulent transport within various parts of the water column. Existing mathematical models of coastal processes generally utilize relatively simple eddy-viscosity concept to parameterize the complex turbulent transport phenomena. When sufficient data exist to establish the validity of the assumed eddy coefficients in the subject models, the model predictions for a particular application can give reasonable results. However, the required site-specific parameter tuning severely limits the predictability of eddy-viscosity models when little data exist and parameters must be extrapolated from much different flow situations. Moreover, turbulent quantities (e.g., shear stresses) computed by the eddy-viscosity models are often inaccurate due to the inherent model assumption that turbulence is always at local equilibrium condition. The lack of proper physics is why eddy-viscosity model often fails to faithfully simulate highly oscillatory and density-stratified flow situations which are often encountered in coastal waters.

This paper introduces a turbulent transport model (often called "second-order closure model") which allows accurate predictions of coastal processes when data is unavailable or hard to obtain. The basic turbulent transport model (4, 17, 18) retains the dynamic equations of the second-order turbulent correlations which affect the mean flow variables. The added physics contained in the second-order closure model allows direct computation of many of the turbulent transport phenomena without resorting to ad-hoc fixes. Following a brief description of the turbulent transport model,this paper presents some recent model simulations of various coastal processes including: turbulent wave boundary layer, current-wave interaction within the bottom layer, mixed layer dynamics and wind-driven currents.

*Senior Consultant, Aeronautical Research Associates of Princeton,Inc. P. O. Box 2229, Princeton, NJ 08540 U. S. A.

2. A SECOND-ORDER CLOSURE MODEL OF TURBULENT TRANSPORT

The second-order closure model of turbulent transport as described herein has been originally developed by Donaldson and his colleagues at A.R.A.P. The model consists of dynamic equations for the mean flow variables as well as the second-order turbulent correlations (e.g., $\overline{u_i u_j}$, $\overline{u_i \rho}$, and $\overline{\rho\rho}$). Models are developed for the unresolved third-order correlations appearing in the second-order correlation equations. Model constants are derived from analyzing a wide class of flow situations and remain invariant for new applications. As such, the model is often termed as an invariant model.

2.1 MODEL EQUATIONS

The model equations of motion for an incompressible fluid in the presence of both a gravitational and a Coriolis body force, with the mean variables denoted by capitals and the turbulent fluctuations by lower-case, may be written in general tensor notation as follows:

$$\frac{\partial U_i}{\partial t} + U_j \frac{\partial U_i}{\partial x_j} = -\frac{\partial \overline{u_i u_j}}{\partial x_j} - \frac{1}{\rho}\frac{\partial P}{\partial x_i} + g_i \frac{(\Theta - \Theta_0)}{\Theta_0} - 2\epsilon_{ijk}\Omega_j U_k \tag{1}$$

$$\frac{\partial U_i}{\partial x_i} = 0 \tag{2}$$

$$\frac{\partial \Theta}{\partial t} + U_j \frac{\partial \Theta}{\partial x_j} = -\frac{\partial \overline{u_j \theta}}{\partial x_j} \tag{3}$$

$$\begin{aligned}\frac{\partial \overline{u_i u_j}}{\partial t} + U_k \frac{\partial \overline{u_i u_j}}{\partial x_k} &= -\overline{u_i u_k}\frac{\partial U_j}{\partial x_k} - \overline{u_j u_k}\frac{\partial U_i}{\partial x_k} + g_i \frac{\overline{u_j\theta}}{\Theta_0} + g_j \frac{\overline{u_i\theta}}{\Theta_0} \\ &\quad - 2\epsilon_{ikl}\Omega_k \overline{u_l u_j} - 2\epsilon_{jlk}\Omega_l \overline{u_k u_i} \\ &\quad + 0.3\frac{\partial}{\partial x_k}\left(q\Lambda\frac{\partial \overline{u_i u_j}}{\partial x_k}\right) - \frac{q}{\Lambda}\left(\overline{u_i u_j} - \delta_{ij}\frac{q^2}{3}\right) - \delta_{ij}\frac{q^3}{12\Lambda}\end{aligned} \tag{4}$$

$$\begin{aligned}\frac{\partial \overline{u_i\theta}}{\partial t} + U_j \frac{\partial \overline{u_i\theta}}{\partial x_j} &= -\overline{u_i u_j}\frac{\partial \Theta}{\partial x_j} - \overline{u_j\theta}\frac{\partial U_i}{\partial x_j} + g_i \frac{\overline{\theta^2}}{\Theta_0} - 2\epsilon_{ijk}\Omega_j \overline{u_k\theta} \\ &\quad + 0.3\frac{\partial}{\partial x_j}\left(q\Lambda\frac{\partial \overline{u_i\theta}}{\partial x_j}\right) - \frac{0.75q}{\Lambda}\overline{u_i\theta}\end{aligned} \tag{5}$$

$$\frac{\partial \overline{\theta^2}}{\partial t} + U_j \frac{\partial \overline{\theta^2}}{\partial x_j} = -2\overline{u_j\theta}\frac{\partial \Theta}{\partial x_j} + 0.3\frac{\partial}{\partial x_j}\left(q\Lambda\frac{\partial \overline{\theta^2}}{\partial x_j}\right) - \frac{0.45q\overline{\theta^2}}{\Lambda} \tag{6}$$

$$\begin{aligned}\frac{\partial \Lambda}{\partial t} + U_i \frac{\partial \Lambda}{\partial x_j} &= 0.35\frac{\Lambda}{q^2}\overline{u_i u_j}\frac{\partial U_i}{\partial x_j} + 0.75q + 0.3\frac{\partial}{\partial x_i}\left(q\Lambda\frac{\partial \Lambda}{\partial x_i}\right) \\ &\quad - \frac{0.375}{q}\left(\frac{\partial q\Lambda}{\partial x_i}\right)^2 + \frac{0.8}{q^2}q_i\frac{u_i\theta}{\Theta_0}\end{aligned} \tag{7}$$

where x_i are coordinate axes, t is time, U_i, U_j, U_k are the mean velocity components, u_i, u_j, u_k are the fluctuating velocity components, ρ is density, Θ and θ are mean and fluctuating temperatures, q is total fluctuating velocity, Λ is turbulent macroscale, δ_{ij} is Kronecker

delta, ε_{ijk} is alternating tensor, Ω is earth's rotation.

In a first-order closure (or eddy viscosity) model, only the first three equations for the mean variables are resolved. The second-order correlations $\overline{u_i u_j}$ and $\overline{u_j \theta}$ appearing in the mean equations are parameterized as the products of eddy coefficients and the mean gradients, $\partial U_i/\partial x_j$ and $\partial \Theta/\partial x_j$ respectively. The most complete second-order closure model, on the other hand, retains all the dynamic equations for the Reynolds stresses $\overline{u_i u_j}$, the heat fluxes $\overline{u_j \theta}$, and the temperature variance $\overline{\theta^2}$. To close the system, a dynamic equation for the turbulent macroscale Λ is introduced. It should be pointed out that many of the terms in the second-order correlation equations do not require any modeling. These include the turbulent production terms, the buoyancy terms, and the Coriolis terms. The third-order correlation and pressure correlation terms appearing in the original Renyolds stress equations have been modeled as a diffusion term and a tendency toward isotropy term. Model constants for the diffusion term, the tendency toward isotropy term, the dissipation term, and other modeled terms have been determined from analyzing a wide class of flow situations (13) and remain fixed for any new applications.

The complete second-order closure model as described by Equations (1) through (7) has been applied to simulate various atmospheric, oceanic, and laboratory problems of practical importance. The ability of the model to simulate a variety of flow situations with the same set of model constants has been successfully demonstrated. Simplified versions of the second-order closure model have also been formulated by retaining the dynamic equations for only part of the second-order correlation variables. For example, the quasi-equilibrium version retains the dynamic equations for q^2 and Λ, while neglecting the diffusion and time evolution terms in other correlation equations. Such an approximation is valid so long as the turbulent time scale Λ/q is small compared to the mean flow time scale, and is being incorporated into a three-dimensional coastal current model(18).

Most of the following model applications utilize the one-dimensional version of the complete second-order closure model. Multi-dimensional versions of the second-order closure model have been utilized in numerous past and present applications, e.g., the detailed dynamics of wakes behind blunt bodies (5) and flow within the core of a tornado (14).

3. TURBULENT WAVE BOUNDARY LAYER

Detailed measurements in turbulent wave boundary layers are scarce. Johnson and Carlsen (9) measured the detailed flow within an oscillating water tunnel with a fixed rough bottom. In their Test I, an 8.39 sec wave with a maximum mean free stream velocity of 2 to 2.22 m/sec and a nearly sinusoidal time variation was imposed on a water depth of 23 cm. Vertical profiles of ensemble-averaged horizontal velocity within the water tunnel were measured at 15° intervals throughout several wave cycles. Multi-layered eddy-viscosity models (10,6,3) and time-varying eddy-viscosity models (8,21) were developed to achieve reasonable simulation of the mean flow variables measured

by Jonsson and Carlsen. Considerable efforts were spent in arriving at the "proper" eddy-viscosity formulation needed to yield good fit of the mean flow data. Using the complete second-order closure model, Sheng (17) successfully simulated Jonsson and Carlsen's turbulent wave boundary layer. Very good agreement was found between the simulated and measured mean velocity, phase lag and shear stress. In addition, model results revealed the transient behavior of a thin classic logarithmic layer modulated by the time-periodic pressure gradient. For simplicity, however, Sheng (17) assumed a sinusoidal free-stream velocity of 2 m/sec amplitude. In the present paper, based on harmonic analysis of the measured data, the following free-stream velocity is used:

$$U_f = A_1 + \sum_{i=2}^{13} \left\{ A_1 \cos\left[(i-1)\,\theta \right] + B_i \sin\left[(i-1)\,\theta \right] \right\} \qquad (8)$$

where A_i and B_i are coefficients determined from the harmonic analysis of Jonsson and Carlsen's free stream velocity. The boundary conditions for the mean and turbulent variables are basically the same as in Sheng (17).

The mean flow profiles at ϕ=0°, 45°, 90°, 135° are shown in Figure 1(a), while those at ϕ=180°, 225°, 270°, 315° are shown in Figure 1(b). Excellent agreement between the computed and measured data is apparent at all levels and all times. A slight mid-level velocity overshoot at peak free-stream velocity, which was found in the earlier results of Sheng (17), is now eliminated.

Vertical profiles of the Reynolds stress $-\overline{\rho uw}$ are shown in Figures 2(a) and 2(b). Excellent agreement between the computed and measured results is found at ϕ=0° and 180°, while the worst agreement is found at ϕ=90° and ϕ=270°. This is because Jonsson and Carlsen's Reynolds stresses were not measure directly, but were computed indirectly from the mean flow data via the following equation:

$$\frac{\tau}{\rho} = - \int_d^z \frac{\partial}{\partial t} \left(U_f - U \right) dz \qquad (9)$$

where d corresponds to τ=0 and was taken to be 17 cm. The Reynolds stresses calculated from Equation (9) are very sensitive to the numerical evaluation of the r.h.s., i.e., accuracy of time derivative and vertical profile of the mean velocity. The mean velocities were only measured at 15° intervals. Hence, one expects error in τ to be the smallest when time variation of mean velocity is the smallest ($\phi \sim 0°$ and 180°)while error is the largest when time variation of mean velocity is the largest ($\phi \sim 90°$ and 270°). This explains the discrepancy found in Figure 2. In this regard, the second-order closure model can be used to guide the design of laboratory experiments by pointing out the needed temporal and spatial resolutions of data. Jonsson and Carlsen also calculated the eddy-viscosity values from

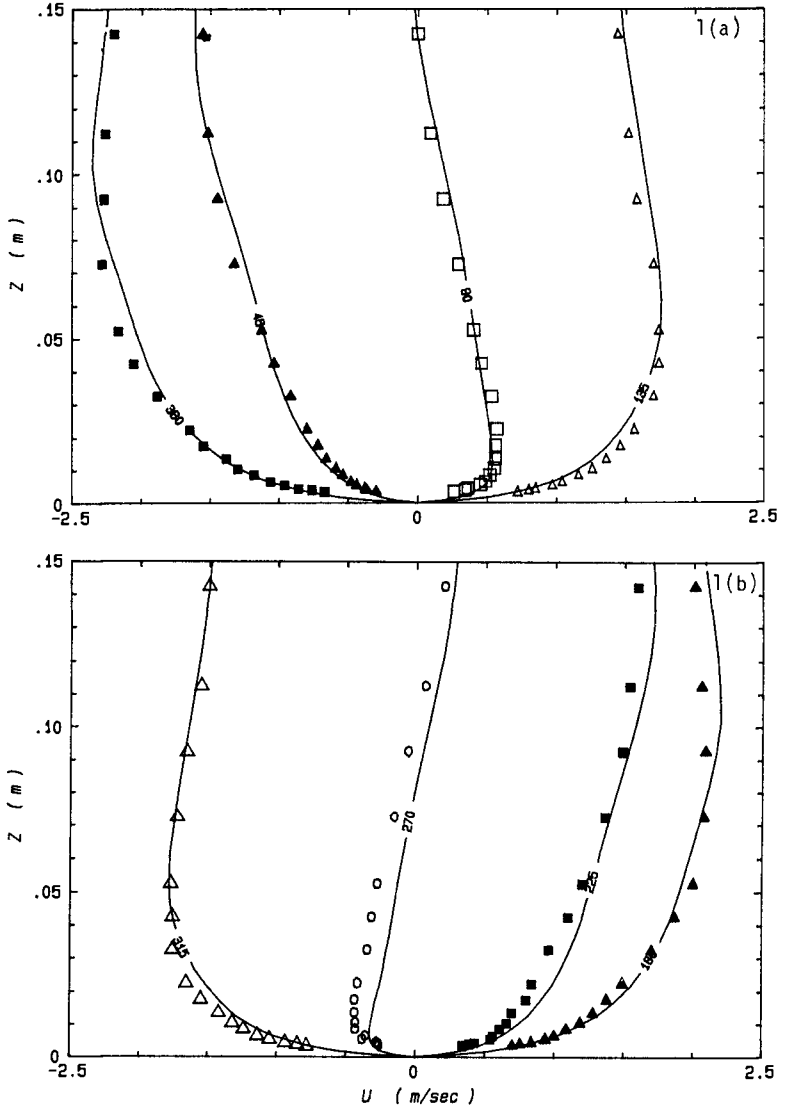

FIGURE 1. Mean velocity vs height in Jonsson and Carlsen's turbulent wave boundary layer (———: model results, symbols: data): (a) at ϕ=0°, 45°, 90°, 135°; (b) at ϕ=180°, 225°, 270°, 315°).

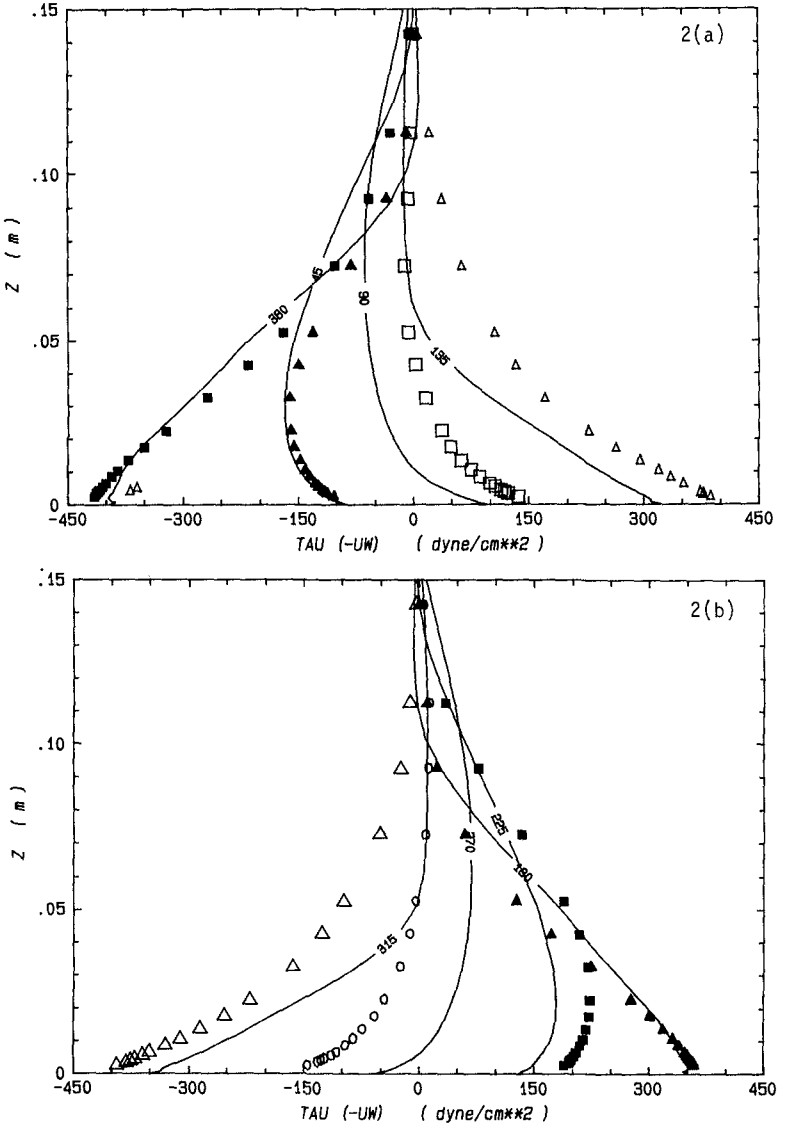

FIGURE 2. Reynolds stress vs height in Jonsson and Carlsen's turbulent wave boundary layer (——: model results, symbols: data): (a) at ϕ=0°, 45°, 90°, 135°; (b) at ϕ=180°, 225°, 270°, 315°).

the calculated shear stresses and vertical gradients of the measured mean velocities. The resulting eddy viscosities are ill-behaved and often have negative values. Attempt to formulate an eddy viscosity model based on these ill-behaved eddy-viscosity values may lead to good fit of mean flow data, but will not provide physical insight of the turbulent transport processes.

Figure 3 presents the temporal variation of U_f, U_{1cm}, τ_{bottom}, $\partial p/\partial x$ and z_{log} (thickness of the classic logarithmic layer). A phase lag of approximately 0.4 radians is found between U_f and U_{1cm} (the mean velocity at 1 cm above the bottom). Similar phase lag is also found between U_f and τ_{bottom} (the bottom stress). The pressure gradient $\partial p/\partial x$ balances the time variation of U_f exactly, and obtains maximum absolute value in the neighborhood of ϕ=90° and 270° but is approximately zero at 0° and 180°. The classical logarithmic layer is the layer within which the Reynolds stress $-\overline{uw}$ varies less than 1% from its bottom value, and the log layer thickness lags behind the pressure gradient by approximately 27°. The maximum thickness of the log layer is only 2.5 cm, or 32 times the roughness height z_o. This rigorously computed value is substantially smaller than Jonsson and Carlsen's estimate of 6.3 cm and the fixed wave boundary layer thickness assumed by Grant and Madsen (7) in their current-wave boundary layer model.

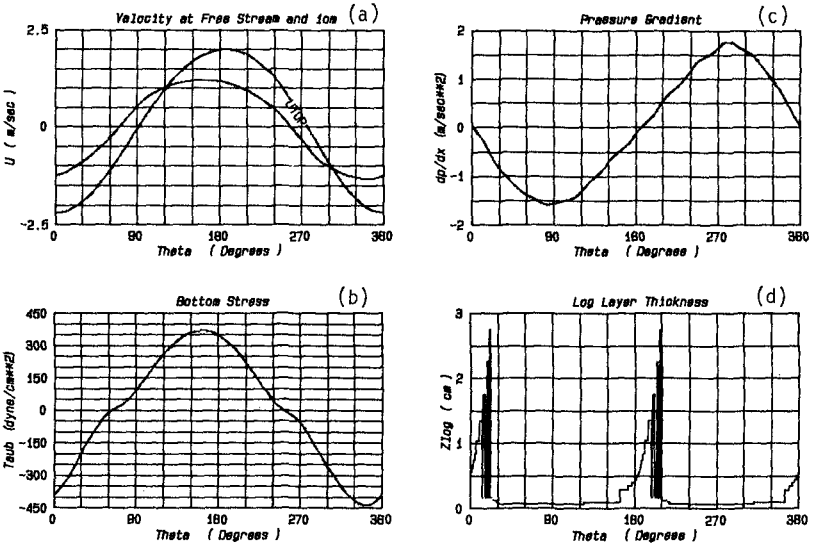

FIGURE 3. Temporal variation of (a) free stream velocity and velocity at 1-cm above the bottom, (b) bottom stress, (c) pressure gradient, and (d) thickness of lag layer over one wave cycle in simulated JC's turbulent wave boundary layer.

4. TURBULENT WAVE BOUNDARY LAYER UNDER A CNOIDAL WAVE

Waves in coastal waters are often nonlinear in nature,particularly when large sea swells are propagated onto very shallow waters. Linear wave theory is often inadequate to describe the wave under these circumstances and cnoidal wave theory has to be used. Cnoidal wave theory is based on the Korteweg-deVries equation (12) and its solution is basically different from those of higher-order Stoke's wave theories. Turbulent wave boundary layer underneath a cnoidal wave has not been previously investigated. The direct extension of the previously mentioned eddy-viscosity models to such cases is questionable. In the following, we present a simulation of the turbulent wave boundary layer underneath a cnoidal wave by means of the second-order closure model.

In a recent physical model study at CERC, the wave parameters within Humboldt Bay, California due to a 11-sec, 10-ft sea swell propagated from the Northwest were measured. Sharp-crested cnoidal waves were clearly observed over much of the Humboldt Bay. At a nearshore station in the vicinity of Buhne Point, the depth (d) is only 2.65 m, and the wave height (H) is 0.64 m. Values of d/gT^2 and H/gT^2 indicate that cnoidal wave theory should be used. The wave orbital velocities were computed by using the cnoidal wave theory and the linear theory and are shown in Figure 4(a). Based on Kajiura's empirical formula for the bottom friction coefficient underneath a linear wave, the computed bottom stresses over a wave cycle are shown in Figure 4(b). Excessively high bottom stress is found underneath the cnoidal wave.

The turbulent wave boundary layer underneath the cnoidal wave was computed by means of the second-order closure model and considering a water column of 20 cm above the bottom. Figure 5(a) shows the mean velocity profiles over the entire cycle at 45° intervals. The sharp-crested nature of the cnoidal wave is clearly manifested by these velocity profiles. Much of the temporal variation takes place during only half of the wave cycle while little variation is found during the other half cycle. The computed Reynolds stress profiles are shown in Figure 5(b). The Reynolds stresses are generally confined to a layer much thinner than what would be underneath a linear sinusoidal wave. Figure 6 shows the temporal variation of U_f, U_{1cm}, τ_{bottom}, $\partial p/\partial x$ and thickness of the logarithmic layer. Compared to its linear counterpart, the logarithmic layer is thinner during the fast half cycle but somewhat thicker during the slow half cycle. The maximum bottom shear stress as shown in Figure 6 is little over 100 dyne/cm^2, a value substantially less than the 180 dyne/cm^2 computed by using Kajiura's empirical formula for sinusoidal wave. More detailed computation of the cnoidal wave within the Humboldt Bay can be found in Sheng (20).

5. CURRENT WAVE INTERACTION WITHIN THE BOTTOM BOUNDARY LAYER

Using an eddy-viscosity model, Grant and Madsen (7) produced a theoretical analysis of combined current and wave flow over a rough boundary, predicting an increase in apparent bed roughness and bottom shear stress when waves are superimposed on the current. Similar models and qualitative results have been produced by others (e.g., 2). As pointed out by Kemp and Simon (11), however, no detailed verification of the above eddy-viscosity models has been made. In addition, these models generally require ad-hoc assumptions on the wave boundary layer.

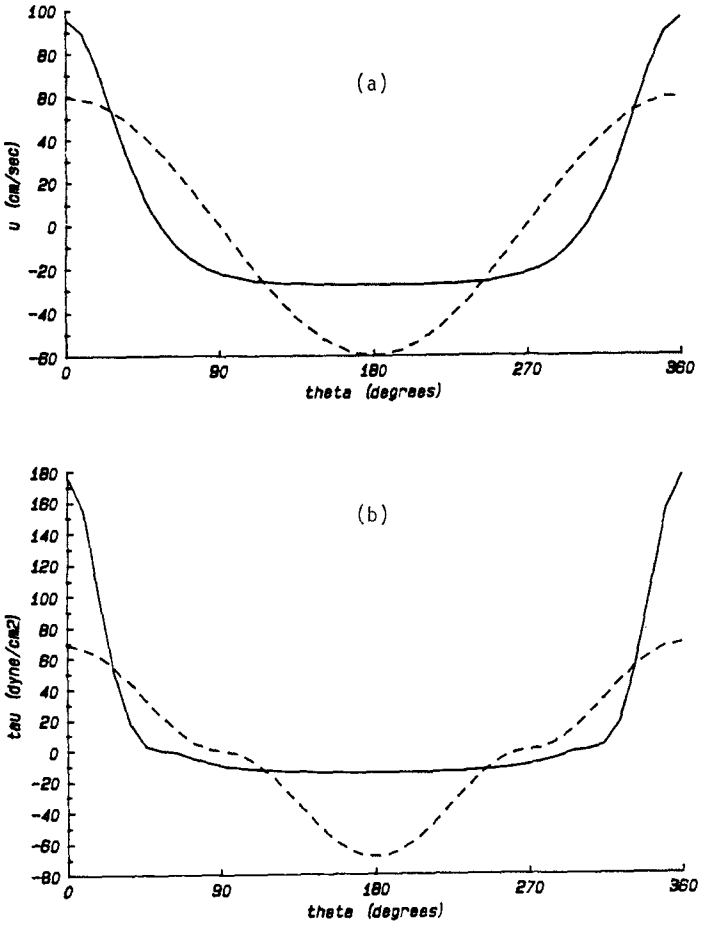

FIGURE 4. Orbital velocity and bottom stress at a station near Buhne Point in Humboldt Bay, CA due to a 11-sec (period) and 10-ft (wave ht.) sea swell propagated from the Northwest (——: cnoidal wave theory, -----: linear wave theory): (a) wave orbital velocity over a wave cycle, (b) bottom stress computed by using Kajiura's empirical formula.

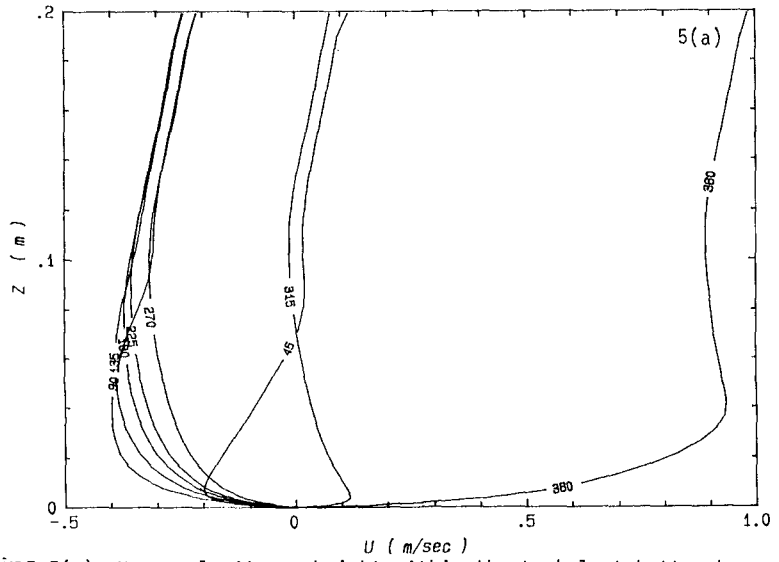

FIGURE 5(a). Mean velocity vs height within the turbulent bottom boundary layer under a cnoidal wave. The profiles are shown at 45° intervals over a wave cycle. Results of second-order closure model.

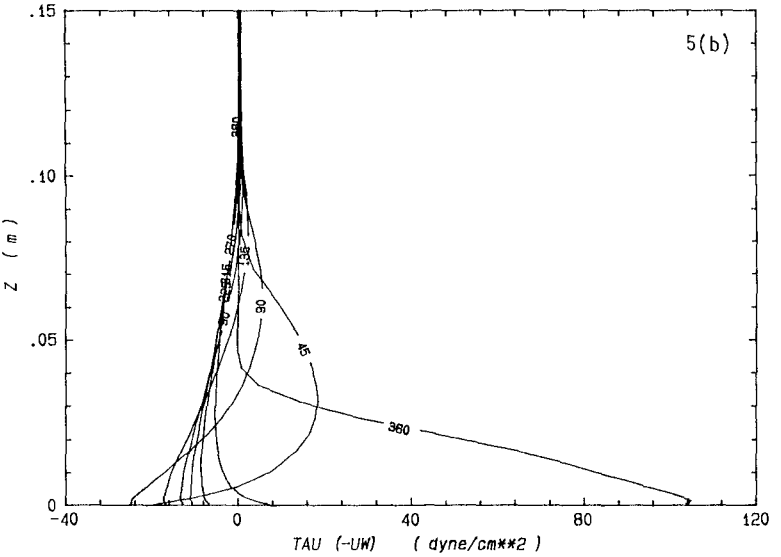

FIGURE 5(b). Reynolds stress vs height within the turbulent bottom boundary layer under a cnoidal wave. The profiles are shown at 45° intervals over a wave cycle.

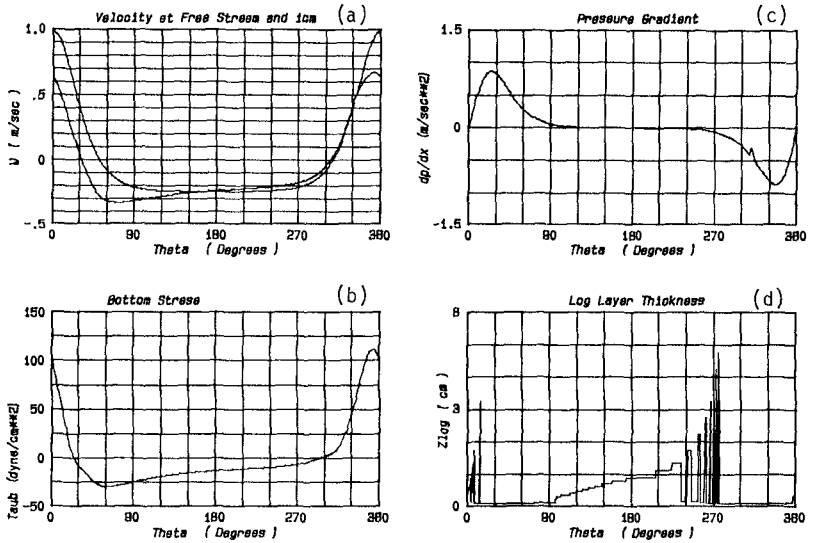

FIGURE 6. Temporal variation of (a) free stream velocity and velocity at 1-cm above the bottom, (b) bottom stress, (c) pressure gradient, and (d) thickness of log layer over one wave cycle in turbulent boundary layer under the cnoidal wave.

In this paper, we present some results on current-wave bottom boundary layer obtained with the second-order closure model. The first simulation is based on some data collected at a CODE site (C3) about 1 km off the California coast. Using z_0=0.2 cm, U_{100cm}=10.21 cm/sec, U_w=6.09 cm/sec, and T_w=13.79 sec, the model computed results (averaged over the wave cycle) within the bottom 1 m are shown in Figure 7. In the absence of any wave, the velocity profile shows a logarithmic variation with depth while the turbulent kinectic energy ($q^2/2$) and Reynolds stress ($-\overline{\rho uw}$) are constant within the bottom boundary layer. When waves are superimposed on the current, the apparent roughness is increased to 0.5 cm while q^2 and $-\overline{uw}$ are increased by more than 50% near the bottom. The increase in $-\overline{uw}$ is less than that produced by Grant and Madsen, which was found to be higher than that determined from the logarithmic velocity profile. If Kajiura's empirical formula was used for the bottom friction coefficient, one finds that the wave-induced bottom stress alone is on the order of 1.3 dyne/cm^2 which is much higher than our combined current-wave result.

The second model simulation is based on the current and wave data at a site in the Mississippi Sound (18) where z_0=0.1 cm, U_{100cm} =20 cm/sec, U_w=20 cm/sec and T_w=2.5 sec. The results shown in Figure 8

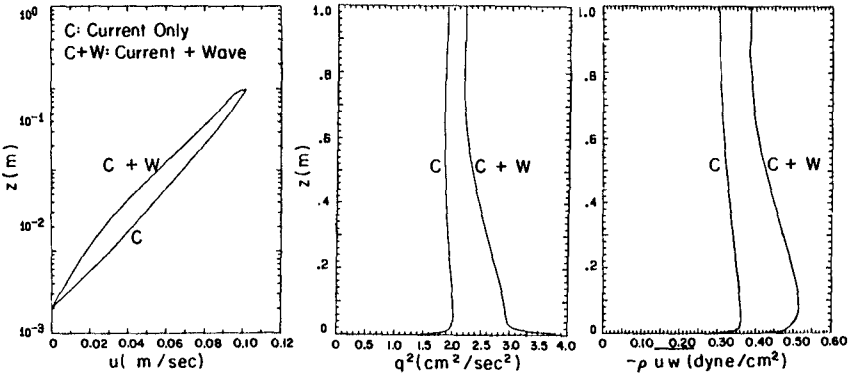

FIGURE 7. Simulated current-wave bottom boundary layer at a CODE site (C3). Vertical profiles of (a) mean velocity, (b) twice the turbulent K.E., and (c) Reynolds stress averaged over the wave cycle. z_o=0.2 cm, U_{100}=10.2 cm/sec, U_w=6.09 cm/sec, T_w=13.79 sec.

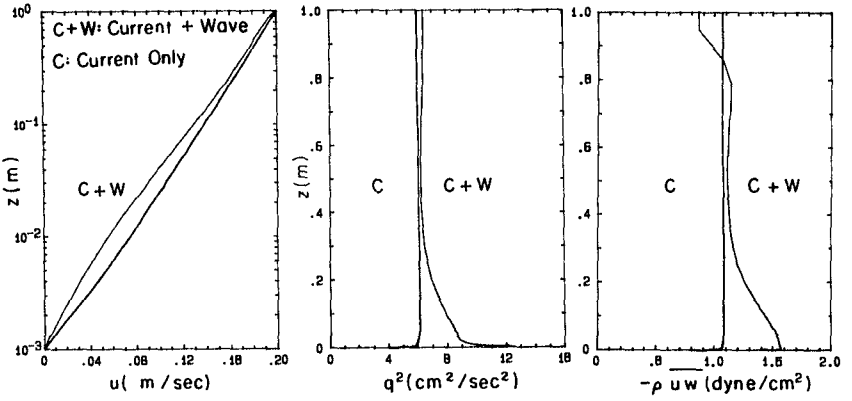

FIGURE 8. Simulated current-wave bottom boundary layer at a site in the Mississippi Sound. Vertical profiles of (a) mean velocity, (b) twice the turbulent K.E., and (c) Reynolds stress averaged over the wave cycle. z_o=0.1 cm, U_{100}=20 cm/sec, U_w=10 cm/sec, T_w=2.5 sec.

indicate the wave boundary layer is relatively thinner compared to the CODE simulation, although more than 50% increase is also found in the q^2 and $-\overline{uw}$ at bottom.

The results presented herein have great engineering implications.

The increased bottom shear stress due to the presence of the wave will lead to enhanced erosion of sediment while the increased turbulent intensity will lead to enhanced mixing of sediment within the water column. In a comprehensive laboratory study of current-wave interaction within the bottom boundary layer, Kemp and Simon (11) found significant phase shift between the turbulent intensity and the bottom stress. Earlier study by van Hoften and Karaki (22) found that presence of the wave may sometimes lead to reduction of the Reynolds stress. To further examine and understand such interesting phenomena, it is essential to use a dynamic turbulent transport model which requires little ad-hoc parameter tuning.

6. MIXED LAYER DYNAMICS

Coastal processes may be affected by density stratification in coastal waters resulting from inhomogeneity in salinity, sediment concentration, and temperature. A predictive model capable of simulating stratified flow situations is highly desirable. Using the second-order closure model, we performed a simulation of the ocean mixed layer measured during MILE (MIxed Layer Experiment) by Miyake (16). Data obtained throughout a 32-day period starting August 2, 1977 exhibited significant temporal variations of the wind stress (between 0 and 5 dynes/cm^2) and heat flux (diurnal heating and cooling cycle) at the ocean site. The model simulation was performed by using the measured temperature profile on August 2, 1977 as initial condition and the measured wind stress and heat flux during the subsequent 32 days as boundary conditions. As shown in Figure 9(a), the simulated mean temperature profile on the 32nd day agrees well with data. So are the simulated surface temperatures throughout the 32-day period in Figure 9(b). Despite the great variability of the weather, the model was able to correctly track the evolution of the thermocline throughout the simulation period.

More recently, a simplified version of the second-order closure model has been applied to simulate the mixed layer dynamics (19). This simplified model is comparable in complexity to the model of Mellor and Durbin (15) but contains more dynamics by allowing a spatially varying turbulence macroscale.

7. WIND-DRIVEN CURRENTS

A simplified three-dimensional version of the second-order closure model was applied to simulate the wind-driven currents in a laboratory flume measured by Baines and Knapp (1). Figure 10 shows the model results at the middle of the flume obtained with the same $U*D/\nu(\sim 51{,}000)$ of the experiment. Both the mean horizontal velocity U and the vertical turbulent velocity w agree very well with measured data. Although the vertical eddy-viscosity A_v was not measured, the simulated peak A_v agree well with an estimated peak value based on the measured turbulence profile and a length scale approximately 20% of the water depth.

8. CONCLUDING REMARKS

This paper presents a brief introduction of a second-order closure model of turbulent transport and recent model applications to simulate various coastal processes of practical importance. Due to the added

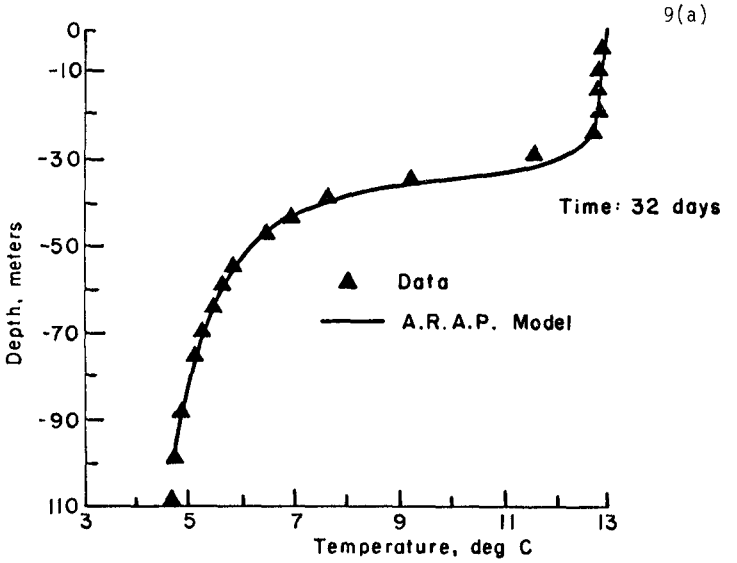

FIGURE 9 (a). Simulated and measured temperature profile at 32 days after the initiation of the MILE ocean mixed layer experiment.

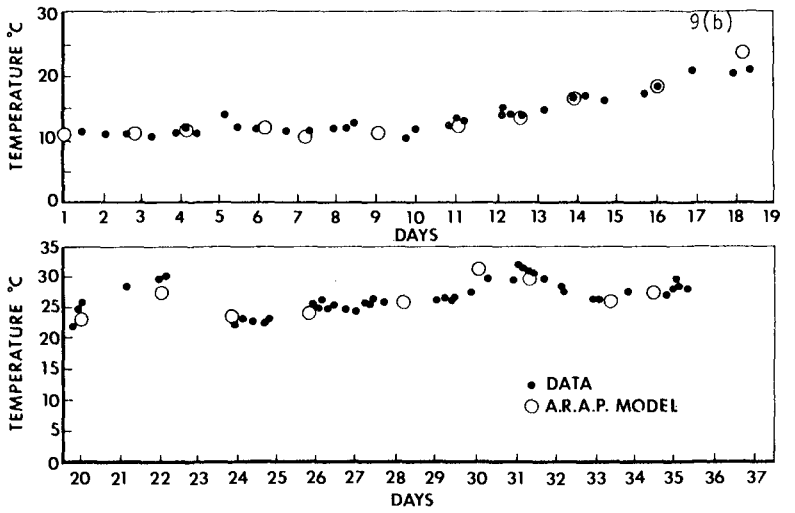

FIGURE 9 (b). Simulated and measured ocean surface temperature during the MILE.

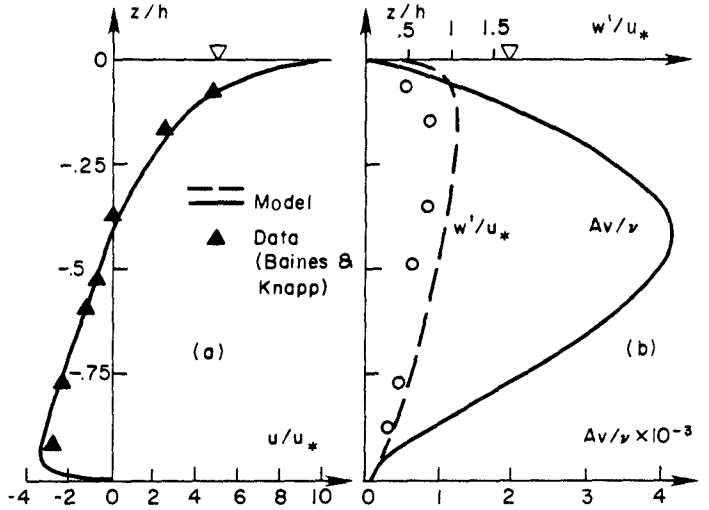

FIGURE 1D. Wind-driven currents in an open channel. Vertical profiles of (a) horizontal velocity, (b) vertical turbulent velocity and eddy viscosity.

physics contained in the model, the model was able to successfully simulate a variety of flow situations without having to perform extensive site-specific tuning of ad-hoc model parameters. Detailed simulations of the turbulent bottom boundary layers and the mixed layer demonstrated that the model may be used to (1) provide detailed understanding of the physical processes, (2) aid the design and interpretation of laboratory/field experiments, and (3) guide the development of first-order closure models (eddy-viscosity models). By combining the turbulent transport model with emerging high-quality laboratory/field data, further understanding on the turbulent current-wave boundary layer can be achieved. Research is also needed to extend the model to study (1) the dispersion of sediments, (2) the hydrodynamic forces on complex structures, and (3) the wave-breaking induced turbulence.

9. ACKNOWLEDGEMENT

This work has been partially supported by the U. S. Army Engineer Waterways Experiment Station under contract DACW 39-8D-C-0087.

10. REFERENCES

1. Baines, W. D. and D. J. Knapp, 1965: "Wind-Driven Water Currents", J. Hyd. Div.,ASCE, 91, No. HY2, pp 205-221.

2. Bakker, W. T. and Th. Van Doorn, 1978: "Near Bottom Velocities in Waves With a Current", Proc. 16th Conf. on Coastal Engineering.

3. Brevik, I., 1981: "Oscillatory Rough Turbulent Boundary Layers", J. Waterways, Port, Coastal and Ocean Div., ASCE, vol. 107, pp 175-188.

4. Oonaldson, C. duP., 1973: "Atmospheric Turbulence and the Oispersal of Atmospheric Pollutants", in AMS Workshop on Micrometeorology, (O.A. Haugen, ed.), Science Press, Boston, pp 313-39D.

5. Donaldson, C. duP., and A. J. Bilanin, 1975: "Vortex Wakes of Conventional Aircraft", AGARDograph, No. 2D4.

6. Grant, W. D. and O. S. Madsen, 1978: "Bottom Friction Under Waves in the Presence of a Weak Current", NOAA Tech Report, ERL-MESA., 150 pp.

7. Grant, W. O. and O. S. Madsen, 1979: "Combined Wave and Current Interaction with a Rough Bottom", J. Geophys. Res., 84, pp 1797-1808.

8. Jonsson, I. G., 1980: "A New Approach to Oscillatory Rough Turbulent Boundary Layers", Ocean Engng., I, pp 1D9-152.

9. Jonsson, I.G., and N. A. Carlsen, 1976: "Experimental and Theoretical Investigations in an Oscillatory Rough Turbulent Boundary Layer", J. Hydr. Res., 14, pp 45-60.

10. Kajiura, K., 1968: "A Model of the Bottom Boundary Layer in Water Waves", Bull Earthq. Res. Inst., 46, pp 75-123.

11. Kemp, P. H., and R. R. Simon, 1982: "The Interaction Between Waves and a Turbulent Current: Waves Propagating with the Current", J. Fluid Mech., vol. 116, pp 227-250.

12. Korteweg, D. J., and G. deVries, 1895: "On the Change of Form of Long Waves Advancing in a Rectangular Canal, and on a New Type of Stationary Waves", Phil. Mag., 5th Series, vol. 39, pp 422-443.

13. Lewellen, W. S., 1977: "Use of Invariant Modeling," in Handbook of Turbulence, vol. 1 (W. Frost, ed.), Plenum Publishing Corp., pp 237-280.

14. Lewellen, W. S., and Y. P. Sheng, 1981: "Modeling Tornado Oynamics", U. S. Nuclear Regulatory Commission Report NUREG/CR-1585, 227 pp.

15. Mellor, G. L., and P. A. Ourbin, 1875: "The Structure and Dynamics of the Ocean Surface Mixed Layer", JPO, 5, pp 718-728.

16. Miyake, M., 1978: "Oceanographic Observations at Ocean Station P", Pacific Marine Science Report 78-1, Institute of Ocean Sciences, Sidney, BC.

17. Sheng, Y. P., 1982: "Hydraulic Applications of a Second-Order Closure Model of Turbulent Transport", in Applying Research to Hydraulic Practice, (P. Smith, ed.), ASCE, pp 106-119.

18. Sheng, Y. P., 1983: "Mathematical Modeling of Three-Oimensional Coastal Currents and Sediment Oispersion", Technical Report CERC-83-2, U. S. Army Engineer Waterways Experiment Station, CE, Vicksburg, MS. Also A.R.A.P. Report No. 458, Princeton, NJ, 288 pp.

19. Sheng. Y. P., 1984a: "A One-Dimensional Ocean Current Model", A. R. A. P. Report No. 523.

20. Sheng, Y. P., 1984b: "Numerical Computation of Current- and Wave-induced erosional forcing within the Humboldt Bay", A.R.A.P. Tech. Memo 84-18, Princeton, NJ.

21. Towbridge, J. and O. S. Madsen, 1984: "Turbulent Wave Boundary Layers", JGR, vol. 89, pp 7989-8007.

22. van Hoften, J. O. A., and S. Karaki, 1976: "Interaction of Waves and a Turbulent Current", Proc. 15th International Conf. Coastal Eng.